(20) Saeda, S.; Yotsuyanagi, J.; Yamaguchi, K. *J. Appl. Polym. Sci.* 1971, *15*, 277.

(21) (a) Carlla, J. M.; Graessley, W. W.; Fetters, L. *J. Macromolecules* 1984, *17*, 2775. (b) A comment made by: Graessley, W. W., private communication.

(22) Green, P. F.; Mills, P. J.; Palmstrom, C. J.; Mayer, J. W.; Kramer, E. *J. Phys. Rev. Lett.* 1984, *53*, 2146.

(23) Lin, Y.-H. *J. Rheol.* 1985, *29*, 605.

(24) Lin, Y.-H. *J. Non-Newtonian Fluid Mech.* 1987, *23*, 163.

(25) See equation (3); M_e^{-1} and M_e^2 are absorbed in the prefactors for η_0 and η_0/M^3, respectively. $G(t)/G_N$ is a universal function of M/M_e (see ref 10). The prefactor of η_0 contains M_e^{-1}, be-

cause η_0 is proportional to G_N. In spite of the fact that the prefactors are functions of M_e, the *line shapes* of η_0 and η_0/M^3 are universal functions of M/M_e, since M_e is a constant (independent of MW).

(26) Berry, G. C.; Fox, T. G. *Adv. Polym. Sci.* 1968, *5*, 261.

(27) Plazek, D. J. *J. Polym. Sci., Polym. Phys. Ed.* 1982, *20*, 729.

(28) See Appendix B of ref 12a.

(29) Allen, V. R.; Fox, T. G. *J. Chem. Phys.* 1964, *41*, 337.

(30) McKenna, G. B.; Hadziioannou, G.; Lutz, P.; Hild, G.; Strazielle, C.; Straupe, C.; Rempp, P.; Kovacs, A. *J. Macromolecules* 1987, *20*, 498.

(31) Graessley, W. W. *J. Polym. Sci., Polym. Phys. Ed.* 1980, *18*, 27.

Computer Simulation of End-Linked Networks: Telechelic Poly(oxyethylene) Cross-Linked with Plurifunctional Isocyanates

K.-J. Lee and B. E. Eichinger*

Department of Chemistry, BG-10, University of Washington, Seattle, Washington 98195. Received May 17, 1988; Revised Manuscript Received August 22, 1988

ABSTRACT: Networks formed from α,ω-dihydroxypoly(oxyethylene) (POE) with plurifunctional isocyanate at various initial polymer volume fractions v_{2c} have been simulated with a computer. Monte Carlo samples of chains based on RIS statistics have been constructed, which yield networks comparable to those based on Gaussian statistics. A detailed study of various types of network imperfections and cycle ranks of the networks is reported. Computer simulation shows that, at a given sol fraction w_s, the Miller–Macosko theory underestimates the extent of reaction by as much as 3.2–8.5%. Moduli are calculated according to the phantom network model, and very good agreement with experiment is found for networks prepared with low molecular weight polymer and with high molecular weight polymer cross-linked at high dilution.

Introduction

The structures of network polymers are important, since the nature of these structures determines the final mechanical properties, such as modulus, dynamical behavior, and ultimate strength. Since techniques for direct investigation of network structures are absent, many efforts have focused on theoretical predictions. Among these are the gelation theory of Flory[1] and Stockmayer,[2] the cascade (stochastic branching) theory,[3] the Miller–Macosko (recursive branching) theory,[4,5] and the rate theory.[6]

The assumptions[1,2] of equal and independent reactivity of like functional groups and no loop formation are not always correct. At high extents of reaction, the remaining unreacted groups in the gel can become isolated from one another. One must also consider intramolecular reactions that lead to the formation of cyclic species in both the sol and the gel portions. Beyond the gel point, the problem of the sol–gel distribution becomes complicated because of the strong competition between intramolecular and intermolecular reactions. The assumption that the sol fraction is acyclic leads to inaccurate gel conditions and distorted distributions, and one must expect that these inaccuracies will persist beyond the gel point. Even in the limit of acyclic pregel systems, postgel intramolecular reactions are found to be important.[7,8] The complexity of postgel reactions renders a comprehensive theoretical treatment rather difficult.

On the other hand, computer simulation can provide valuable information on these reactions. The algorithm that simulates random polycondensation has been well developed in previous work.[9] The advantage of our computer algorithm is the fact that we are able to probe the internal structures of the simulated molecules. Subsequently, the information obtained can give us details of the extent of cyclization, cycle rank, and sol–gel distribu-

tions.[9] The algorithm has been adapted to simulate critical gel points[10] and mechanical properties.[11] Another advantage of the algorithm is that it is easily modified to simulate other types of reactions, such as the end-linking of polyol stars[12] with bifunctional groups or the radiation cure of clastomer networks.[13,14]

The system that is simulated here was studied experimentally by Gnanou, Hild, and Rempp.[15] It is described chemically as $A_2 + B_f$ (ref 15 defines their system as $A_f + B_2$), where A_2 is a telechelic prepolymer with α and ω reactive end groups and B_f ($f = 2, 3, 5, 7, 9$)[15] is a cross-linker with a distribution of functionalities: the mole fractions of the B_f are 0.055, 0.55, 0.17, 0.11, and 0.115, respectively. A code which generates Monte Carlo samples of polymer chains[16-21] based on the rotational isomeric state theory[22] has been written. In these simulations, prepolymers having n skeletal bonds were generated by using both the RIS and the Gaussian distribution of end-to-end distances. Results from the two distributions are compared.

Simulation Procedure

Generation of Reaction Container. The details of end-linking algorithm have been described in a previous work.[9] In the model, prepolymer chains and cross-linkers are randomly distributed in a cubical box whose length L is determined by the equation

$$L = (nM_0N_p/\rho N_a v_{2c})^{1/3} \tag{1}$$

where n is the number of skeletal bonds, M_0 is the average molecular weight of one bond unit, N_p is the number of prepolymer chains, ρ is the density of the prepolymer, N_a is Avogadro's number, and v_{2c} is the volume fraction of polymer during the cross-linking process. The sample chain configurations are generated either by use of a

Gaussian distribution[9] of the end-to-end vector or by a Monte Carlo method[16-21] based on the rotational isomeric state theory.[22]

Gaussian Chain Generation. The distribution of end-to-end distances of the prepolymer chains was generated from random numbers with a Gaussian distribution. The variance of the distribution is given[23] by

$$\sigma^2 = C_n n \bar{l}^2 / 3 \tag{2}$$

where C_n is the characteristic ratio[22] and $\bar{l}$ is the average length of one backbone bond.

Monte Carlo Chain Generation. The polyoxyethylene (POE) chains under investigation are represented as $HO-(CH_2CH_2O)_x-H$, where $x = n/3$. The bond lengths, l_{C-O} and l_{C-C}, are 0.143 and 0.153 nm, respectively.[22,24] Supplements of bond angles[22,24] O-C-C and C-O-C are nearly the same and are taken to be 70°.

The rotational isomeric state theory provides a convenient representation of the spatial configurations of polymer chains. The rotational states are trans (t), gauche plus (g⁺), and gauche minus (g⁻), such states being located at $\phi = 0°$, 120°, and −120°, respectively. The statistical weight matrices[22] applicable to the repeating bonds C-O, O-C, and C-C are U_a, U_b, and U_c, respectively. They are formulated as

$$U_a = \begin{bmatrix} 1 & \sigma & \sigma \\ 1 & \sigma & \sigma\omega \\ 1 & \sigma\omega & \sigma \end{bmatrix} \tag{3a}$$

$$U_b = \begin{bmatrix} 1 & \sigma & \sigma \\ 1 & \sigma & 0 \\ 1 & 0 & \sigma \end{bmatrix} \tag{3b}$$

$$U_c = \begin{bmatrix} 1 & \sigma' & \sigma' \\ 1 & \sigma' & \sigma'\omega \\ 1 & \sigma'\omega & \sigma' \end{bmatrix} \tag{3c}$$

where $\sigma = \exp(-900/RT)$, $\omega = \exp(-350/RT)$, and $\sigma' = \exp(430/RT)$, with RT in cal/mol. The elements of the statistical weight matrices characterize the conformations of bond pair $(i - 1, i)$, so that the rotational states of the bound i are indexed on the columns in the order t, g⁺, g⁻, and those of the preceding bond $i - 1$ are indexed on rows in the same order. In this simulation, the temperature[25] is 60 °C. At this temperature, parameters for the statistical weight matrices are $\sigma = 0.26$, $\sigma' = 1.90$, and $\omega = 0.60$.

The statistical weight matrices can be converted into conditional probability matrices by the procedure described by Flory.[22] A conditional probability $q_{\xi\eta;i}$ is the probability that bond i will be in state η given that bond $i - 1$ is in state ξ. The conditional probability matrices corresponding to eq 3 have elements whose rows sum to unity. They are

$$Q_a = \begin{bmatrix} 0.676 & 0.162 & 0.162 \\ 0.724 & 0.174 & 0.102 \\ 0.724 & 0.102 & 0.174 \end{bmatrix} \tag{4a}$$

$$Q_b = \begin{bmatrix} 0.696 & 0.152 & 0.152 \\ 0.821 & 0.179 & 0.000 \\ 0.821 & 0.000 & 0.179 \end{bmatrix} \tag{4b}$$

$$Q_c = \begin{bmatrix} 0.236 & 0.382 & 0.382 \\ 0.280 & 0.453 & 0.267 \\ 0.280 & 0.267 & 0.453 \end{bmatrix} \tag{4c}$$

The conformation of each bond of a polymer chain is de-

termined by conditional probabilities based on random numbers. Details of the procedure have been given by Hill and Stepto,[16] by Yoon and Flory,[17] and by DeBolt and Mark.[21]

Once the rotational states (t, g⁺, g⁻) of a chain have been determined in this way, the end-to-end vector **r** is calculated by[26]

$$\mathbf{r} = \mathbf{A}_1 \left(\prod_{i=2}^{n-1} \mathbf{A}_i \right) \mathbf{A}_n \tag{5}$$

In this equation, $\mathbf{A}_1$, $\mathbf{A}_i$ and $\mathbf{A}_n$ are matrices defined by

$$\mathbf{A}_1 = [\mathbf{T} \ \mathbf{I}]_1 \tag{6a}$$

$$\mathbf{A}_i = \begin{bmatrix} \mathbf{T} & \mathbf{I} \\ 0 & 1 \end{bmatrix}_i \tag{6b}$$

$$\mathbf{A}_n = \begin{bmatrix} \mathbf{I} \\ 1 \end{bmatrix}_n \tag{6c}$$

where $\mathbf{I}_i = \text{col} \ (l_i, 0, 0)$ and $\mathbf{T}_i$ is the operator matrix[22] which transforms a vector in reference frame $i + 1$ to its representation in reference frame i, by premultiplication.

The number of end-to-end vectors that were generated was determined by the size of the simulation. After having determined all of the end-to-end vectors, they were positioned at random in the imaginary reaction container with directions determined by a random unit vector generator.[27]

End-Linking Process. The number of cross-linking agents N_c is given by

$$N_c = 2r_s N_p / \bar{f} \tag{7}$$

where r_s is the stoichiometric ratio of the cross-linker's functional units (B) to the number of functional units on chains (A), and $\bar{f}$ is the functionality of the cross-linking reagent, here equal to the average functionality of the plurifunctional isocyanate mixture. In order to facilitate comparisons with the results of Gnanou et al.,[15] a distribution of functionalities of cross-linkers consistent with the experiments was constructed, again by using a random number generator.

Bond formation between A and B is controlled by the following conditions: (a) the group A is unreacted, (b) there is an unreacted B group on the cross-linker, (c) the distance between A and B falls within a capture radius which controls the extent of reaction, and (d) there are no other A groups closer to the given B. During the end-linking process, the program records the details of connectivity for all molecules and finds the connected components by the SPANFO subroutine.[28] The gel is sorted from the sol, and the various connected components are examined to determine the number of dangling ends and loops in various topological classes.

For a given static configuration of chains, the capture radius is increased step by step to span a range of extents of reaction. At high conversions, only one large component and several small components are generated, and these are readily identified as gel and sol, respectively.

Results and Discussion

Simulations were run for five different molecular weights of POE with our model of the plurifunctional isocyanate (Desmodur N 75)[15] in the stoichiometric ratios r_s shown in Tables II and III. Values of parameters are $M_0 = 14.68$ g/mol, $\bar{l} = 0.146$ nm, $\rho = 1.21$ g/cm³,[25] and characteristic ratio[22] $C_n = 3.8$, 3.9, and 4.0 for $M_n = 1010$ and 1810 and $M_n \geq 3400$, respectively. In this simulation, 10 000 primary chains were generated either with use of the Gaussian distribution[16] or by Monte Carlo methods based on RIS
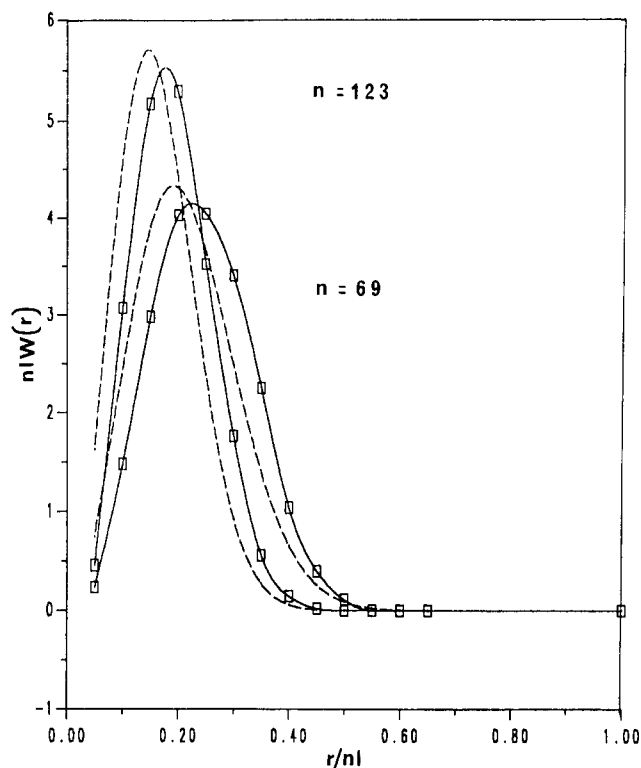
Figure 1. End-to-end distance distribution functions obtained from the RIS theory for POE chains having $n = 69$ and 123 at 60 °C (solid curves). The Gaussian distributions for $n = 69$ and 123 are shown by the dashed curves.

weights. Quoted results are averages over at least four configurations for each set of parameters. Previous studies[9,10] have shown that edge effects are imperceptible if more than about 5000 primary chains are generated.

Distribution Functions. The end-to-end distances r of the primary POE chains generated by use of the RIS based Monte Carlo method were grouped into 20 bins. The proportion of chains in each bin is plotted against r/nl to obtain the non-Gaussian distribution $W(r)$, as shown by the solid curves in Figure 1. Depicted are the results for 10 000 POE chains having 69 ($M_n = 1010$) and 123 ($M_n = 1810$) skeletal bonds, respectively.

Figure 1 also displays Gaussian distribution functions as dashed curves, which were calculated from

$$nl(r) = (3/2\pi\langle\rho^2\rangle_0)^{3/2}4\pi\rho^2 \exp(-3\rho^2/2\langle\rho^2\rangle_0) \quad (8)$$

where $\rho = r/nl$ and $\langle\rho^2\rangle_0 = C_n/n$. The investigation of Mark and Curro[19] on poly(dimethylsiloxane) (PDMS) showed that the Gaussian distribution overestimates the probability for larger values of r compared with the RIS for 20 and 40 skeletal bonds of PDMS. Figure 1 shows that, unlike PDMS, the RIS curves of POE are roughly approximated by the Gaussian distribution. This may be attributed to the fact that we are investigating longer chains. The values of C_∞ for POE and PDMS are 4.0 and 6.43, respectively.[22] The difference between the C_∞ values is primarily due to the differences of bond angles[29] in the two chains, that is, POE and PDMS are almost equally flexible.

Network Imperfections. There are two major types of network defects. Loops are formed when the two active ends of a primary chain connect to the same cross-linker. Dangling ends are attached to the network at only one end. Both types of defective primary chains are elastically inactive; they do not deform with strain. Our computer program[9] identifies not only the structures of small molecules in the sol fraction, it also finds irregularities such
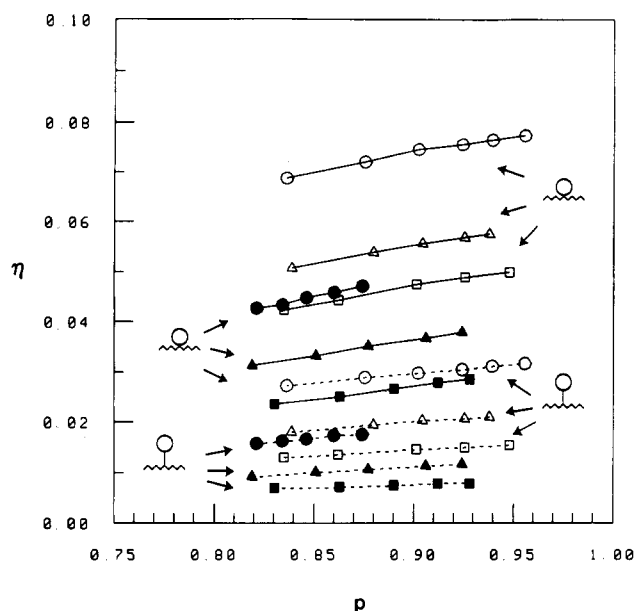

Figure 2. Plots of inner loop (solid lines) and dangling loop (dashed lines) populations versus the extent of reaction for different molecular weights and for various volume fractions. $M_n = 5600$ (filled symbols): $v_{2c} = 0.19$ (●), 0.32 (▲), and 0.48 (■). $M_n = 1010$ (open symbols): $v_{2c} = 0.24$ (○), 0.40 (△), and 0.56 (□).

as dangling ends, single loops, two-chain loops, and double-edge circuits in the gel. Since the probability of forming two-chain loops and double-edge circuits in the gel is very small, dangling ends and loop defects are the focus of this section. The population η of network imperfections is defined in terms of the ratio of the number of fragments of a particular type that occur to the number of primary chains incorporated into the gel.

Simulations were performed for $M_n = 1010$, 1810, 3400, 5600, and 8300 and for various volume fractions v_{2c}. For clarity, only the results for $M_n = 1010$ and 5600 are shown in the figures (open and filled symbols, respectively.) Different volume fractions are represented by the symbols: circles, triangles, and squares. Three types of dangling ends and two types of loop defects are reported here. Unless otherwise specified, depicted results are from simulations using the Gaussian approximation.

The proportions of the two types of loop defects, dangling loops and inner loops, are shown in Figure 2. The jagged lines in the caricatures represent the remainder of the network. The junction that is incorporated in a loop may be unsaturated if the functionality f of the cross-linker is greater than 3 (dangling loop) or 4 (inner loop). Figure 2 shows how the populations of loop defects depend on the extent of reaction. If a dangling loop's junction is unsaturated, it can be converted to an inner loop as the extent of reaction increases. Since the mole fraction of the cross-linkers with $f = 3$ is 0.55, some junctions incorporated into dangling loops are saturated. Therefore, the slopes of the curves for dangling loops in Figure 2 remain nearly constant instead of decreasing (see Figure 2, dashed lines), and those for the inner loops in Figure 2 increase slightly (see Figure 2, solid lines). Previous studies[9] on PDMS in the bulk showed that the extent of intramolecular reaction depends on the molecular weight of the primary chains, with more loops being formed the lower the molecular weight is. Ilavský and Dušek[30] and Stepto[31] have shown that in the formation of networks, cyclization is enhanced by high dilution. Figure 2 also shows that for lower molecular weight and higher dilution the proportion of loops increases. The top solid curve of Figure 2, which has the highest population of inner loops, is for the lowest mo-
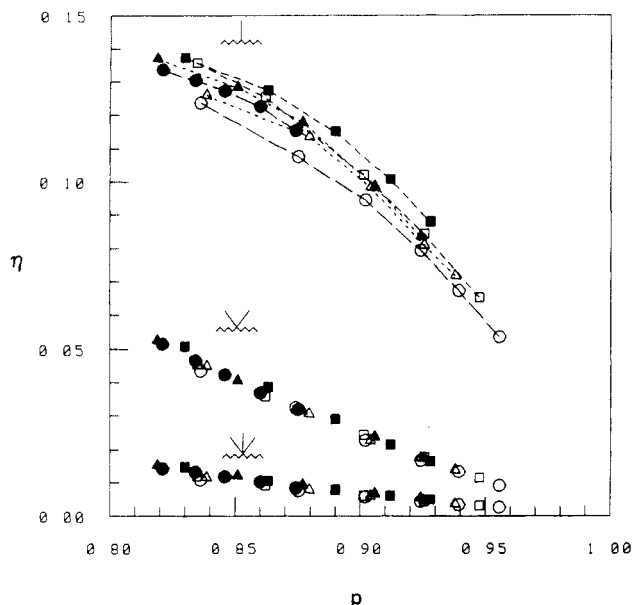
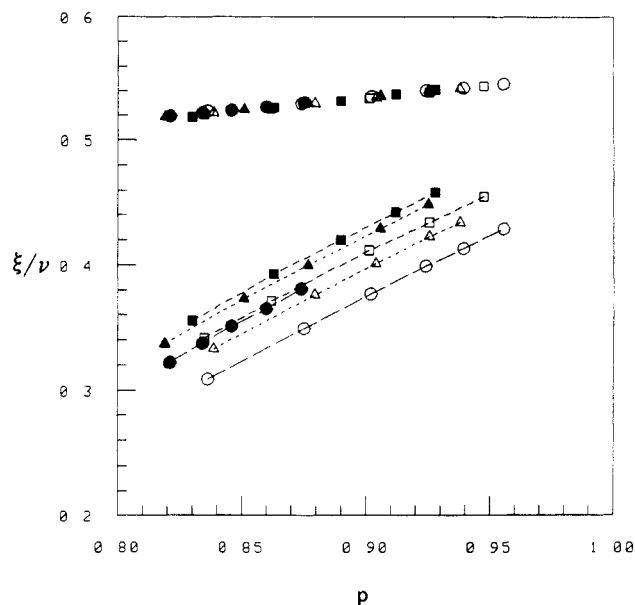**Figure 3.** Populations of I, V, and ψ dangling ends. Symbols are the same as those of Figure 2.

Figure 4. Cycle ranks per chain obtained from these simulations. Symbols are the same as those of Figure 2. The largest values (without connecting curves) are obtained from these simulations with use of eq 9–11 that make use of the Scanlan–Case definition of active chains. The short-dashed line with filled symbols (■) depicts results for M_n = 5600 and v_{2c} = 0.48. The lowest curve (long-dashed line) with open symbols (○) is for M_n = 1010 and v_{2c} = 0.24. The latter results make use of our alternative definition of active chains and junctions.

lecular weight (M_n = 1010) and the highest dilution (v_{2c} = 0.19). These results are similar to previous work[10] on PDMS.

Results for dangling ends are shown in Figure 3. The symbols used in this figure were introduced in previous work;[9] the three types of dangling ends are represented as "I", "V", and "ψ", and the remainder of the network is indicated by jagged lines (see Figure 3). All of the three types of dangling ends may connect to either a saturated junction or an unsaturated one, according to the functionality f of the cross-linker to which they connect. For example, if f is greater than 3, type I might be connected to an unsaturated junction. In Figure 3, the proportions η of the three types of dangling ends are plotted against the extent of reaction p for different molecular weights of the prepolymers and for various initial polymer volume fractions v_{2c}. It is clear that types V and ψ are favored at low extents of reaction, and the proportion of them falls to zero faster than does that of type I at higher conversion. As the reaction proceeds, types V and ψ are converted into type I, and the rate of formation of the latter is proportional to the population of types V and ψ. Type I disappears by attachment of the free end to a cross-linker, which converts it into a loop or an active chain. The populations of types V and ψ are independent of molecular weight and initial polymer volume fractions, while the percentage of type I is lower for low molecular weight and for low reaction concentration (see Figure 3, long-dashed line). Previous studies[9,10] and Figure 2 show that there is a higher probability for intramolecular reactions to form single loops as the molecular weight of the prepolymer is reduced or as the dilution of the reaction is increased. During the conversion of types V and ψ in low molecular weight and high dilution systems, loops are more apt to form, which reduces the chances for their conversion to type I.

Cycle Rank. According to the phantom network model, the elastic modulus of a network is determined by the cycle rank of the graph representing the network structure. The cycle rank is the number of cuts required to reduce the network to an acyclic graphic or tree.[32] The relation between the elastic free energy and cycle rank has been developed by Flory.[33] For a macroscopic loopless network, the cycle rank ξ is defined as the difference $\xi = \nu - \mu$ between the number of effective chains ν and the number

of effective junctions μ of any functionality $f \geq 2$. In these simulations, we have adopted the same definitions as in previous work[9] to evaluate the cycle rank. An effective junction is a vertex of a graph whose degree is greater than one, and an effective chain is attached to two different effective junctions.[34] Chains that are dangling ends and loops are excluded from the count of effective chains, while the junctions to which those chains are attached are included as effective junctions.

Using this counting scheme, the cycle ranks can be readily deduced from the results of the simulations. Cycle ranks per chain ξ/ν are plotted against the extent of reaction p for two different molecular weights and various volume fractions v_{2c} in Figure 4. Symbols used are the same as those of Figure 2 and 3. The differences between the values of ξ/ν shown in Figure 4 are due to loop defects, since loop formation is dependent on molecular weights and reaction concentrations, as discussed above.

Scanlan[35] and Case[36] have defined an active junction as a B molecule that is connected by at least three paths to the network, and an active chain is terminated by active junctions at both its ends. Gnanou et al.[15] have used the Miller–Macosko theory[4,5,37] to determine the number of active chains ν_a and active junctions μ_a according to the equations

$$\nu_a = \sum_{f=3,5,7,9} [B_f]_0 \sum_{i=3}^{f} (i/2)P(x_i) \tag{9}$$

and

$$\mu_a = \sum_{f=3,5,7,9} [B_f]_0 \sum_{i=3}^{f} P(x_i) \tag{10}$$

where $[B_f]_0$ is the initial concentration of the cross-linking agent and $P(x_i)$ is the probability that a B_f group chosen at random is a junction of functionality i. The cycle rank ξ_a based on the Scanlan–Case criteria and the Miller–Macosko theory is
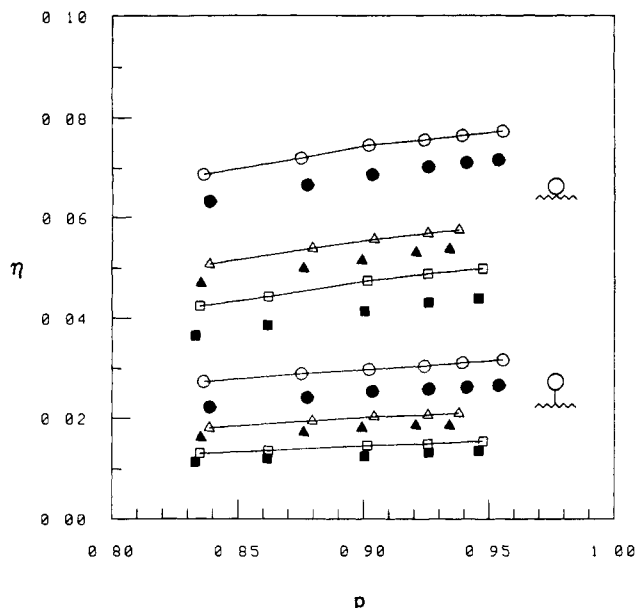
$$\xi_a = \nu_a - \mu_a \tag{11}$$

Figure 5. Plots of inner loop and dangling loop populations versus the extent of reaction for two different methods for generating primary chains: Gaussian (open symbols) and RIS (filled symbols). The results are obtained for M_n = 1010 with v_{2c} = 0.24 (O), 0.40 (△), and 0.56 (□).

Figure 6. Comparison of Gaussian and RIS configuration statistics on the populations of I, V, and ψ dangling ends. Symbols are the same as those of Figure 5.

To compare our simulations with the calculations of Gnanou et al.,[15] we have obtained values of $[B_f]_0 P(x_i)$ for use in eq 9 and 10 from the simulations by keeping track of the number of cross-linkers of degree i which are incorporated into the network. The cycle ranks per chain ξ_a/ν_a obtained from these simulations according to eq 9–11 are also presented in Figure 4. It is clear that the quantity ξ_a/ν_a is not sensitive to the molecular weights and dilutions, because the Miller–Macosko theory neglects intramolecular reactions.

Queslel and Mark[38] have derived the two equations

$$\mu = \frac{\mu_a}{3p - 2} \tag{12}$$

and

$$\nu = \nu_a\left(\frac{p}{3p - 2}\right) \tag{13}$$

for an imperfect trifunctional network. According to this treatment, a perfect network (p = 1.0) is one for which μ = μ_a and ν = ν_a. It is obvious that for high conversions and high functionality networks ($f \geq 3$); ν is nearly equal to ν_a. Also, the number of difunctional junctions μ_2 approaches zero, since the junctions become saturated. Flory[34] and Graessley and Pearson[39] have shown that $\nu - \mu = \nu_a - \mu_a$. In our simulations to model the Gnanou et al.[15] experiments, the percentage of difunctional cross-linkers is 5.5%. The discrepancy between ξ/ν and ξ_a/ν_a at p = 1.0 that is evident on extrapolation of the curves to the axis in Figure 4 arises from loop defects and difunctional junctions μ_2.

Comparisons of the Gaussian with the RIS Theory. Figures 5–7 show the influence of different methods for generating the primary chain configurations on the various defects and the cycle rank. Results for primary chains with M_n = 1010 generated by the Gaussian approximation and by the Monte Carlo–RIS method are given by open and filled symbols, respectively.

To understand these results, it is useful to return to Figure 1, which shows that the Gaussian distribution overestimates the probability of occurrence of small values of r compared with the RIS-generated distributions.
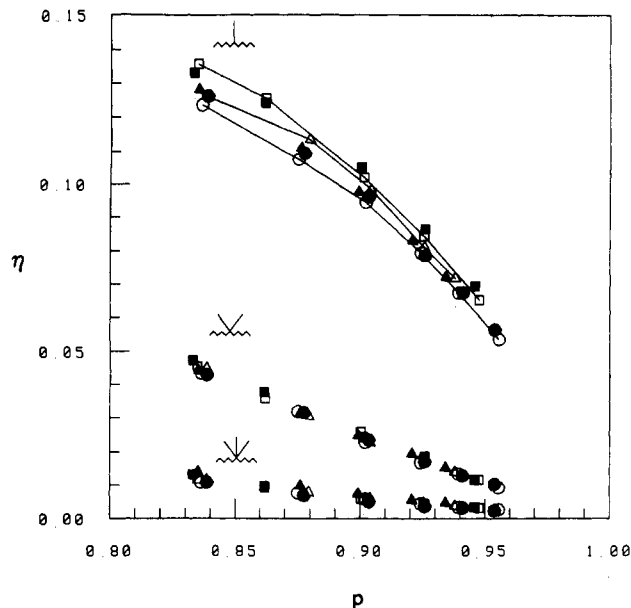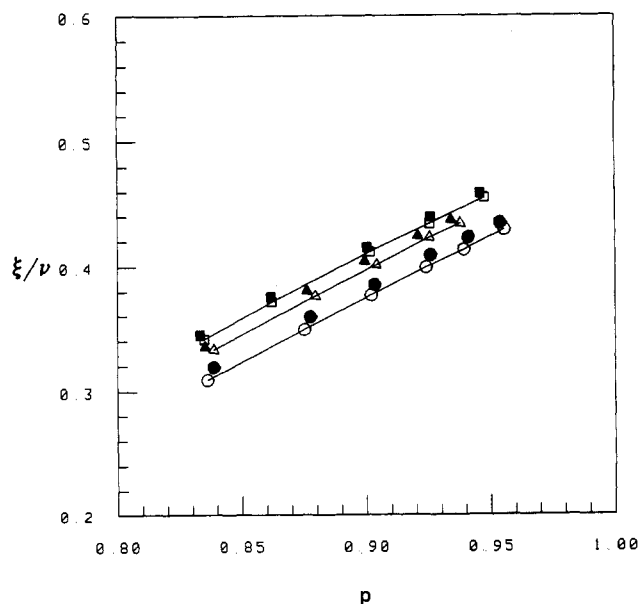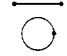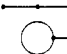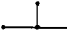

Figure 7. Cycle rank per chain obtained from simulations with $\xi = \nu - \mu$. Symbols are the same as those of Figure 5; the comparison is for Gaussian and RIS configurations.

Results for the proportion of loops that are formed using the two different chain distributions are given in Figure 5 for three different values of v_{2c}. It is seen that the proportion of loops is ~0.5% greater for the Gaussian than for the RIS distribution. This is because the primary chains generated by the Gaussian have a higher probability of having a smaller end-to-end distance, which favors the formation of loops.

Figure 6 shows related results for dangling ends for the same three values of v_{2c}. Despite the premise that an enhanced probability for loop formation should reduce the chance of converting types V and ψ to type I, there are no perceptible population differences between these results for the two distributions in comparable cases. This may be attributed to the small differences (~0.5%) between the loop statistics. A more likely explanation is that the number of intramolecular reactions is much the same for the two distributions, so that larger cycles compensate for

Table I
Dominant Sol Constituents

x-mer	graph	$10^2 w_x^a$	$10^2 w_x^b$
1	———	1.22	1.20
	◯	0.15	0.06
2	●——●—	0.06	0.09
	◯——	0.32	0.17
3	⊥	0.06	0.10
others		0.29	0.18

$^a M_n = 1010$, $v_{2c} = 0.24$, $p = 0.955$, and $w_s = 2.1\%$. $^b M_n = 5600$, $v_{2c} = 0.48$, $p = 0.928$, and $w_s = 1.8\%$.

Table II
Results from Simulations and Miller–Macosko Theory:[15]
Prepolymer Chains Generated by the Gaussian and the RIS Theory

M_n	$w_s, \%$	v_{2c}	r_s	p^a	ξ/v^a	$\xi_a/v_a^{a,c}$	ref	p^b	ξ/v^b
1010	2.1	0.24	1.04	0.955	0.429	0.546	d	0.893	0.518
				0.954	0.434	0.545	e		
	2.4	0.40	1.04	0.938	0.434	0.541	d	0.880	0.514
				0.934	0.437	0.541	e		
	1.6	0.56	1.04	0.948	0.455	0.544	d	0.905	0.522
				0.946	0.458	0.543	e		
1810	2.1	0.22	1.04	0.953	0.442	0.546	d	0.893	0.515
				0.951	0.440	0.545	e		
	1.3	0.35	1.04	0.959	0.462	0.548	d	0.914	0.525
				0.960	0.466	0.546	e		
	0.5	0.53	1.05	0.980	0.490	0.551	d	0.944	0.551
				0.978	0.489	0.549	e		

^{a} This work. ^{b} Reference 15. ^{c} Calculated according to eq 9–11. ^{d} Prepolymer chains generated from the Gaussian distribution. ^{e} Prepolymer chains generated with RIS theory.

the lower proportion of loops. This would tend to make the fraction of chains in dangling ends insensitive to the details of two distributions. Figure 6 shows that types V and ψ are not sensitive to the distribution of chain vectors.

Figure 7 shows cycle ranks per chain ξ/v obtained by the two methods for three different v_{2c}. It is obvious that the small differences between the cycle ranks per chain at the same values of v_{2c} are due to differences in the loop defects that are seen in Figure 5.

Comparisons of Simulations with the Miller–Macosko Theory. The compositions of several constituents (graphs) in the sol for $M_n = 1010$ ($v_{2c} = 0.24$) and 5600 ($v_{2c} = 0.48$) are listed in Table I, where w_x is the weight fraction of the x-mer. Results for other systems have been omitted for clarity. There are two types of molecules in the sol: trees and cyclic molecules. The treelike molecules are predominantly linear monomer, dimer, and branched trimer. The cyclic molecules found in substantial concentrations are cyclic monomer and tadpole dimer. The most abundant molecule, the linear monomer, constitutes ~58% of the weight of the sol for $M_n = 1010$ and ~67% for $M_n = 5600$.

To aid comparisons, data in the first four columns of Tables II and III are the same as those of the experiment.[15] The data in column 5 of Tables II and III are the extents of reaction p obtained from this simulation by adjusting the capture radius to give the same sol fraction w_s as those obtained experimentally.[15] The extents of reaction p derived by the Miller–Macosko theory[4,5,15] (branching theory) are entered into column 9 of Table II and column 8 of Table III. The Miller–Macosko theory utilizes the sol fraction w_s which is experimentally available to determine the extent of reaction p. This theory, which assumes that only treelike molecules exist in the sol, overestimates the number of unreacted chains. As previous work[9,10] and Table I show, there are some cyclic molecules in the sol

Table III
Results from Simulations with Gaussian Distribution of End-to-End Vectors and Miller–Macosko Theory[15]

M_n	$w_s, \%$	v_{2c}	r_s	p^a	ξ/v^a	$\xi_a/v_a^{a,c}$	p^b	ξ/v^b
3400	5.3	0.20	1.05	1.880	0.373	0.528	0.843	0.481
	1.5	0.33	1.04	0.947	0.459	0.544	0.908	0.523
	1.7	0.50	1.04	0.932	0.453	0.539	0.903	0.516
5600	5.2	0.19	1.04	0.874	0.381	0.529	0.845	0.471
	2.2	0.32	1.03	0.925	0.448	0.540	0.892	0.528
	1.8	0.48	1.03	0.928	0.458	0.541	0.900	0.517
8300	3.4	0.18	1.06	0.906	0.411	0.533	0.870	0.500
	5.1	0.31	1.02	0.855	0.382	0.525	0.847	0.500
	1.3	0.47	1.05	0.940	0.464	0.540	0.913	0.512

^{a} This work. ^{b} Reference 15. ^{c} Calculated according to eq 9–11.

fraction, and the actual extent of reaction is increased on their account. It is apparent from columns 5 and 9 of Table II and columns 5 and 8 of Table III that the assumption that all molecules in the sol fraction are acyclic causes the extent of reaction to be underestimated by as much as 3.2–8.5%. (This range should be 2.7–6.2% according to ref 15, but eq 13 of ref 15 neglects the weight fraction of cross-linkers, and this causes the extent of reaction p to be too high by ~2% on the average.[55])

Data in column 6 of Tables II and III are the cycle ranks per chain ξ/v calculated with use of the definitions of effective chains and effective junctions (above). The cycle ranks per chain ξ_a/v_a in column 7 of Tables II and III are calculated from this simulation on the basis of eq 9–11, whereas those in the last columns of Tables II and III are the cycle ranks per chain derived by the branching theory.[15] The differences between column 6 and column 7 of Table II and III are due to the loop defects and difunctional junctions μ_2, the latter of which includes both difunctional cross-linkers and high functionality cross-linkers that are unsaturated (see Figure 4). Values in the last columns of Tables II and III are derived from the branching theory, which underestimates the extent of reaction by several percent. As a result, the values in the last columns are lower than those of column 7 of Tables II and III, which are based on the direct determination of junction functionality from the simulations.

Phantom Network. The phantom model is due to James and Guth.[40] In this model, the network is composed of Gaussian chains which may move freely through one another. The junctions of the network fluctuate around their mean positions, which are determined by the macroscopic dimensions. The displacements of these mean positions are linear (affine) in the macroscopic strain, but the fluctuations about the mean are independent of the strain. The elastic free energy of a Gaussian phantom network was rederived by Flory[33] and is given by

$$\Delta A_{el}(ph) = (\xi kT/2)(\lambda_1^2 + \lambda_2^2 + \lambda_3^2 - 3) \qquad (14)$$

where λ_1, λ_2, and λ_3 are extension ratios along the principal axes of the strain relative to the undeformed state of reference obtained during cross-linking and ξ is the cycle rank of the network.

Using a procedure similar to the derivation of the modulus for the affine model,[1,41] the modulus E_G derived from eq 14 with respect to the swollen, unstretched phantom network is

$$E_G = (\xi/V_0)RTv_2^{1/3} \qquad (15)$$

where V_0 is the volume of the reference state obtained when the reaction is carried out in the bulk and v_2 is the volume fraction of the network in the swollen state at which the stress–strain behavior is measured. If the network is formed in solution, one must consider the

Table IV
Experimental[15] and Simulation Theory Elastic Moduli for M_n = 1810 and 5600

M_n	w_s, %[a]	v_{2c}[a]	v_2[a]	$10^2\xi^b/V^0$	$10^{-5} \times E_G{}^a$	$10^{-5} \times E_G{}^c$	$10^{-5} \times E_{G,exptl}{}^a$
1810	1.00	0.160	0.095	3.843	6.00	8.01	7.05
	1.30	0.356	0.129	9.034	10.68	15.9	11.6
	0.50	0.525	0.189	15.52	18.4	27.4	26.5
	1.30	0.612	0.214	16.78	22.8	29.3	32.1
	0.30	1.00	0.254	30.90	31.0	48.5	45.0
5600	5.20	0.190	0.043	1.065	1.20	1.61	1.01
	2.20	0.320	0.078	2.463	2.76	3.81	4.32
	1.82	0.480	0.096	3.859	4.24	5.59	6.14
	0.97	0.570	0.130	5.038	5.94	7.63	14.1
	0.20	1.00	0.214	10.38	12.4	15.4	29.6

[a] Reference 15. [b] Cycle ranks (in mol/L) calculated according to $\xi/V^0 = (v - \mu)/V^0$. [c] Modulus (in dyn/cm^2) calculated according to eq 16 by using ξ/V^0 from column 5 and T = 298.15 K.[46]

volume fraction v_{2c} of polymer during cross-linking. Equation 15 is then expressed by[42,43]

$$E_G = (\xi/V^0)RTv_2{}^{1/3}v_{2c}{}^{-1/3} \qquad (16)$$

where V^0 is the reference volume that obtains at the time of cross-linking. In this simulation model, V^0 is the volume of the imaginary container.

Experimental moduli are available[15] for networks prepared from prepolymers with M_n = 1810 and 5600 at concentrations ranging from high dilution to the bulk. Simulations were performed for these different systems, and the results were used in conjunction with the phantom network theory to give the elastic moduli shown in Table IV. In order to facilitate comparisons with experiment, the data in the first four columns of Table IV are the same as those of Gnanou et al.[15] Column 5 contains cycle ranks obtained from these simulations using the equation $\xi = v - \mu$. The entries in column 6 are the same as those given by Gnanou et al.;[15] they were calculated with the use of eq 16 and the Miller–Macosko theory. Column 7 contains our predictions for the moduli, as calculated from the cycle ranks in column 5 together with eq 16. The last column contains the experimental moduli.[15]

Table V shows results for the percentage of prepolymer chains that is converted to elastically active chains according to the Miller–Macosko theory[15] and our simulations. For the same reaction conditions (first three columns), the percentage conversions obtained from the Miller–Macosko theory (column 6) is lower than that found from simulations (column 8). As the reaction proceeds, values of the ratio μ/v decrease because the cross-linkers in the network become saturated; i.e., for a given number of crosslinkers, there are more chains v in the gel component at high conversion than there are at low conversion. The value of μ/v decreases with increasing conversion on this account. In these simulations, the extents of reaction in the last column approach p = 1.0. This causes the cycle ranks per unit volume obtained from simulations to be higher than those given by the branching theory.[15] Therefore, the values of the moduli in column 7 are larger than those in column 6 of Table IV and are closer to the experimental values in the last column of Table IV.

To see how good the agreement is with the experimental moduli, it is useful to estimate the uncertainty in the experimental measurements. The experimental moduli[15,33,42-47] were calculated from

$$E_{G,expt} = \frac{\sigma}{\alpha - \alpha^{-2}} \qquad (17)$$

where σ is the stress per unit of cross-sectional area of the swollen sample and α is the uniaxial compression ratio. It

Table V
Results from Simulations and the Miller–Macosko Theory:[15] Percentage Conversion of Prepolymer Chains to Elastically Active Chains

M_n	w_s, %	v_{2c}	$[POE]_0{}^a$	$[v]^b$	Y_c, %[c]	v^d	Y_c, %[e]	p^f
1810	1.00	0.160	0.081	0.057	70.4	8040	80.4	0.970
	1.30	0.356	0.178	0.120	67.4	8354	83.5	0.959
	0.50	0.525	0.262	0.196	74.8	8950	89.5	0.980
	1.30	0.612	0.305	0.258	84.6	8556	85.6	0.956
	0.30	1.00	0.497	0.386	77.7	9196	91.7	0.981
5600	5.20	0.190	0.036	0.017	47.2	6849	68.5	0.874
	2.20	0.320	0.060	0.036	60.0	7979	79.8	0.925
	1.82	0.480	0.092	0.058	63.0	8152	81.5	0.928
	0.97	0.570	0.109	0.078	71.6	8623	86.2	0.948
	0.20	1.00	0.198	0.161	81.3	9294	93.0	0.978

[a] Initial concentrations (in mol/L) of the POE chains from ref 15. [b] Concentrations (in mol/L) of the elastically active chains from ref 15. [c] Percentage conversion from column 4 to column 5. [d] This work, number of effective chains. [e] This work, percentage conversion of 10 000 primary chains to effective chains (column 7). [f] The extents of reaction obtained from these simulations.

should be noted that the uncertainty in $\alpha - \alpha^{-2}$ varies with α and is very large when α is ~ 1.0. We assume the values[47,48] for α ranged from 0.50 to 0.70. For an apparatus[47] calibrated to 0.1 mm, the uncertainty in $\alpha - \alpha^{-2}$ should fall between 3.4% and 10.0%, respectively. One also must consider errors in the measurement of the base area of the gel cylinder and the force F exerted on the sample. The experimental investigations of shear moduli of poly(oxypropylene triols) carried out by Fasina and Stepto[49] demonstrated that the departures from Gaussian behavior fall between 7.3% and 29.0%. On the basis of these estimates of error, the values in column 7 of Table IV for M_n = 1810 are judged to be in good agreement with the experimental moduli in the last column.

Table IV also shows that for M_n = 5600 and for v_{2c} = 0.19, 0.32, and 0.48, the values of the simulation-theory moduli E_G calculated from eq 16 agree quite nicely with the experimental modulus $E_{G,expt}$. For the two highest v_{2c} the experimental values are about twice as large as the calculated. The Flory–Erman theory[50-52] predicts a crossover from phantom to affine behavior as the constraints on the junctions become more severe. For a tetrafunctional network, this crossover increases the modulus by a factor of 2. The average functionality of the Desmodur N 75 used in the experiments is 4.4,[15] and therefore the factor of 2 is comprehensible in these terms. Whether this interpretation is more correct than one based either on Langley-type trapped entanglements[53,54] or on an as yet obscure relation between topology and modulus remains to be seen. At the very least, our results admit an alternative interpretation of the experimental data.

Conclusions

The polyurethane system studied by Gnanou, Hild, and Rempp[15] has been simulated with the aid of the computer. The main objective of this work has been to compare our simulation-based interpretation of the experimental data with that deriving from the Miller–Macosko theory. A computer simulation model that allows intramolecular reactions to occur is a powerful tool to observe sol–gel distributions and to explore the structures of the networks. Neglect of the effect of cyclics in the sol causes the branching theory to underestimate the extent of reaction by several percent. Loop defects are formed as a result of intramolecular reactions between topological neighboring groups. These defects do not vanish at high conversion, and as a result they reduce the cycle rank in proportion to the number of primary chains reacting to form loops. It is found that differences between two

methods (Gaussian and RIS) for generating the primary chain configurations are very small. Computed cycle ranks have been used with theoretical models to calculate elastic moduli. It is found that these simulations give good agreement for networks prepared from M_n = 1810 at various volume fractions v_{2c} or from M_n = 5600 at v_{2c} = 0.19, 0.32, and 0.48 but underestimate the moduli for prepolymer M_n = 5600 prepared at higher polymer concentrations by a factor of approximately 2.

Registry No. (POE)(Desmodur N75) (copolymer), 88842-45-9.

References and Notes

(1) Flory, P. J. *Principles of Polymer Chemistry*; Cornell University Press: Ithaca, NY, 1953.
(2) Stockmayer, W. H. *J. Chem. Phys.* **1943** *11*, 45; **1944**, *12*, 125.
(3) Gordon, M. *Proc. R. Soc. London, Ser. A* **1962**, *268*, 240.
(4) Macosko, C. W.; Miller, D. R. *Macromolecules* **1976**, *9*, 199.
(5) Miller, D. R.; Macosko, C. W. *Macromolecules* **1976**, *9*, 206.
(6) Stepto, R. F. T. In *Developments in Polymerization-3*; Haward, R. N., Ed.; Applied Science: Barking, Essex, 1982; Chapter 3.
(7) Stepto, R. F. T. In *Biological and Synthetic Polymer Networks*; Kramer, O., Ed.; Elsevier Applied Science Publishers: London, 1988; Chapter 10.
(8) Stepto, R. F. T. *Acta Polym.* **1988**, *39*, 61.
(9) Leung, Y. K.; Eichinger, B. E. *J. Chem. Phys.* **1984**, *80*, 3877, 3885.
(10) Shy, L. Y.; Leung, Y. K.; Eichinger, B. E. *Macromolecules* **1985**, *18*, 983.
(11) Neuburger, N. A., Eichinger, B. E. *J. Chem. Phys.* **1985**, *83*, 884.
(12) Shy, L. Y.; Eichinger, B. E. *Br. Polym. J.* **1985**, *17*, 200.
(13) Shy, L. Y.; Eichinger, B. E. *Macromolecules* **1986**, *19*, 2787.
(14) Galiatsatos, V.; Eichinger, B. E. *J. Polym. Sci., Polym. Phys. Ed.* **1988**, *26*, 595.
(15) Gnanou, Y.; Hild, G.; Rempp, P. *Macromolecules* **1987**, *20*, 1662.
(16) Hill, J. L.; Stepto, R. F. T. *Trans. Faraday Soc.* **1971**, *67*, 3202.
(17) Yoon, D. Y.; Flory, P. J. *J. Chem. Phys.* **1974**, *61*, 5366.
(18) Flory, P. J.; Chang, V. W. C. *Macromolecules* **1976**, *9*, 33.
(19) Mark, J. E.; Curro, J. G. *J. Chem. Phys.* **1983**, *79*, 5705.
(20) Mark, J. E.; DeBolt, L. C.; Curro, J. G. *Macromolecules* **1986**, *19*, 491.
(21) DeBolt, L. C.; Mark, J. E. *Macromolecules* **1987**, *20*, 2369.
(22) Flory, P. J. *Statistical Mechanics of Chain Molecules*; Interscience: New York, 1969.
(23) Eichinger, B. E. *J. Chem. Phys.* **1981**, *75*, 1964. Eichinger, B. E.; Martin, J. E. *Ibid.* **1978**, *69*, 4595.
(24) Abe, A.; Mark, J. E. *J. Am. Chem. Soc.* **1976**, *98*, 6468.
(25) Gnanou, Y.; Hild, G.; Rempp, P. *Macromolecules* **1984**, *17*, 945.
(26) Flory, P. J. *Macromolecules* **1974**, *7*, 381.
(27) International Mathematical and Statistical Libraries Inc. (IMSL) Program GGSPH.
(28) Nijenhuis, A.; Wilf, H. S. *Combinatorial Algorithms*; Academic Press: New York, 1975; Chapter 18.
(29) Huglin, M. B.; Stepto, R. F. T. *Makromol. Chem.* **1970**, *132*, 225.
(30) Ilavský, M.; Dušek, K. *Macromolecules* **1986**, *19*, 2139.
(31) Stepto, R. F. T. *Polymer* **1979**, *20*, 1324.
(32) Harary, F. *Graph Theory*; Addison-Wesley: Reading, MA, 1971.
(33) Flory, P. J. *Proc. R. Soc. London, Ser. A* **1976**, *351*, 351.
(34) Flory, P. J. *Macromolecules* **1982**, *15*, 99.
(35) Scanlan, J. *J. Polym. Sci.* **1960**, *43*, 501.
(36) Case, L. C. *J. Polym. Sci.* **1960**, *45*, 397.
(37) Valles, E. M.; Macosko, C. W. *Macromolecules* **1979**, *12*, 673.
(38) Queslel, J. P.; Mark, J. M. *Adv. Polym. Sci.* **1984**, *65*, 135.
(39) Pearson, D. S.; Graessley, W. W. *Macromolecules* **1978**, *11*, 528.
(40) James, H. M.; Guth, E. *J. Chem. Phys.* **1947**, *15*, 669.
(41) Flory, P. J.; Rehner, J. Jr. *J. Chem. Phys.* **1943**, *11*, 521.
(42) Flory, P. J. *J. Chem. Phys.* **1950**, *18*, 108.
(43) Flory, P. J. *Macromolecules* **1979**, *12*, 119.
(44) Dušek, K.; Prins, W. *Adv. Polym. Sci.* **1969**, *6*, 1.
(45) Flory, P. J. *Polymer* **1979**, *20*, 1317.
(46) Macret, M.; Hild, G. *Polymer* **1982**, *23*, 748.
(47) Hild, G. *Makromol. Chem.* **1976**, *177*, 1947.
(48) Donkersloot, M. C. A.; Gouda, J. H.; van Aartsen, J. J.; Prins, W. *Recl. Trav. Chim. Pays-Bas* **1967**, *86*, 321.
(49) Fasina, A. B.; Stepto, R. F. T. *Makromol. Chem.* **1981**, *182*, 2479.
(50) Flory, P. J. *J. Chem. Phys.* **1977**, *66*, 5720.
(51) Erman, B.; Flory, P. J. *J. Chem. Phys.* **1978**, *68*, 5363.
(52) Flory, P. J.; Erman, B. *Macromolecules* **1982**, *15*, 800.
(53) Langley, N. R. *Macromolecules* **1968**, *1*, 348.
(54) Pearson, D. S.; Graessley, W. W. *Macromolecules* **1980**, *13*, 1001.
(55) Dotson, N., private communication.